J. Fluid Mech. (1998), *vol.* 358, *pp.* 245–258. Printed in the United Kingdom

Suboptimal control of turbulent channel flow for drag reduction

By CHANGHOON LEE[1]†, JOHN KIM[1] AND HAECHEON CHOI[2]

[1]Department of Mechanical and Aerospace Engineering, University of California, Los Angeles, CA 90095-1597, USA

[2]Department of Mechanical Engineering, Seoul National University, Seoul, Korea

(Received 13 May 1997 and in revised form 27 October 1997)

Two simple feedback control laws for drag reduction are derived by applying a suboptimal control theory to a turbulent channel flow. These new feedback control laws require pressure or shear-stress information only at the wall, and when applied to a turbulent channel flow at $Re_\tau = 110$, they result in 16–22% reduction in the skin-friction drag. More practical control laws requiring only the local distribution of the wall pressure or one component of the wall shear stress are also derived and are shown to work equally well.

1. Introduction

Recent studies have shown that near-wall streamwise vortices are responsible for high skin-friction drag in turbulent boundary layers. Many attempts aiming at controlling these vortices have been made in order to achieve a skin-friction drag reduction in turbulent boundary layers. Most of such attempts, however, have been *ad hoc*, largely based on physical intuition. The active control by Choi, Moin & Kim (1994), for example, used blowing and suction at the wall that is equal and opposite to the wall-normal component of the velocity at $y^+ = 10$, resulting in as much as 25% reduction in their numerical simulation. This approach, however, is impractical since the required velocity information at $y^+ = 10$ is not normally available. For any practical implementation a control scheme should be based solely on quantities measurable at the wall.

A more systematic approach based on an optimal control theory was proposed by Abergel & Temam (1990). Choi *et al.* (1993) proposed a 'suboptimal' control procedure, in which the iterations required for a global optimal control were avoided by seeking an optimal condition over a short time period. The suboptimal control procedure was successfully applied to control of the Burgers equation. Bewley & Moin (1994) were the first to apply the suboptimal control procedure to a turbulent flow and reported about 17% drag reduction. The procedure developed by Bewley & Moin (1994) still requires velocity information inside the flow in order to solve the adjoint problem, from which a feedback control input was derived. In spite of this obvious drawback, however, the fact that a control theory applied to a turbulent flow resulted in a substantial drag reduction is encouraging, since their control procedure was derived rigorously from a control theory, in which a pre-determined

† Present address: Department of Mechanical Engineering, University of Seoul, Seoul, Korea.

cost functional was minimized. Hill (1993, 1994) derived a control input as a function of the streamwise wall shear only by modeling the near-wall flow with a spanwise velocity growing linearly, and normal velocity growing quadratically, with normal distance from the wall. About 15% drag reduction was obtained from this study. We, however, derive a simple control scheme by minimizing cost functionals that are related to the streamwise vortices, which have been found to be responsible for large local drag in turbulent boundary layers. We also tried to minimize drag directly by having drag itself in the cost functional, but it was not successful (see § 3). The objective of this paper is to demonstrate that a wise choice of the cost functional coupled with a variation of the formulation can lead to a more practical control law.

We present how to choose a cost functional and how to minimize it to yield simple feedback control laws that require quantities measurable only at the wall. One of the laws requires spatial information on the wall pressure over the entire wall and the other requires information, also over the entire wall, on one component of the wall shear stress. We then derive more practical control schemes that only require local wall pressure or local surface shear stress information, and show that they work equally well.

2. Suboptimal procedure

We follow a similar procedure used by Choi *et al.* (1993) and Bewley & Moin (1994). The problem under consideration is a turbulent channel flow, for which the governing equations are the Navier–Stokes and continuity equations with the no-slip boundary condition:

$$\frac{\partial u_i}{\partial t} + u_j \frac{\partial u_i}{\partial x_j} = -\frac{\partial p}{\partial x_i} + \frac{1}{Re} \frac{\partial^2 u_i}{\partial x_j \partial x_j}, \tag{2.1}$$

$$\frac{\partial u_j}{\partial x_j} = 0, \tag{2.2}$$

with

$$u_i|_w = \phi(x, z, t)\delta_{i2}, \tag{2.3}$$

where t is the time, x_1, x_2, x_3 are the streamwise, wall-normal, and spanwise directions respectively, u_i are the corresponding velocity components, p is the pressure, and Re is the Reynolds number, and the control input is the wall-normal velocity at the wall, ϕ.

All variables are non-dimensionalized by the wall shear velocity, u_τ, and the channel half-width, δ. We also use interchangeably x, y, z for x_i and u, v, w for u_i. Periodic boundary conditions are imposed in the streamwise and spanwise directions. The flow rate in the streamwise direction is kept constant, and the drag is measured by the mean pressure gradient necessary to maintain the constant flow rate.

We found that the choice of the cost functional to be minimized is critical in the performance of the control. Since the streamwise vortices have been known to be responsible for large drag in turbulent boundary layers, we tried to choose the cost functional that is directly related to them. This is based on our conjecture that a suitable manipulation of the streamwise vortices would lead to drag reduction. We carefully selected two cost functionals based on our observation of a successful control of Choi *et al.* (1994). As shown in figure 1, Choi *et al.*'s (1994) blowing and suction, which are equal and opposite to the wall-normal velocity component at $y^+ = 10$, effectively suppress a streamwise vortex by counteracting up-and-down

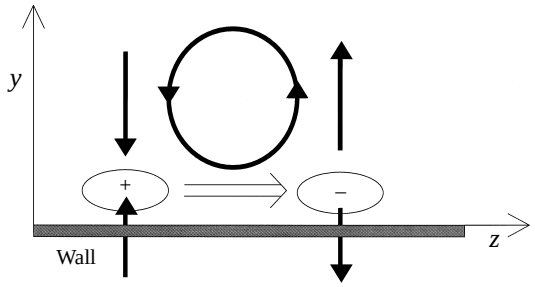

FIGURE 1. Schematic of a pressure field induced by a control based on $y^+ = 10$.

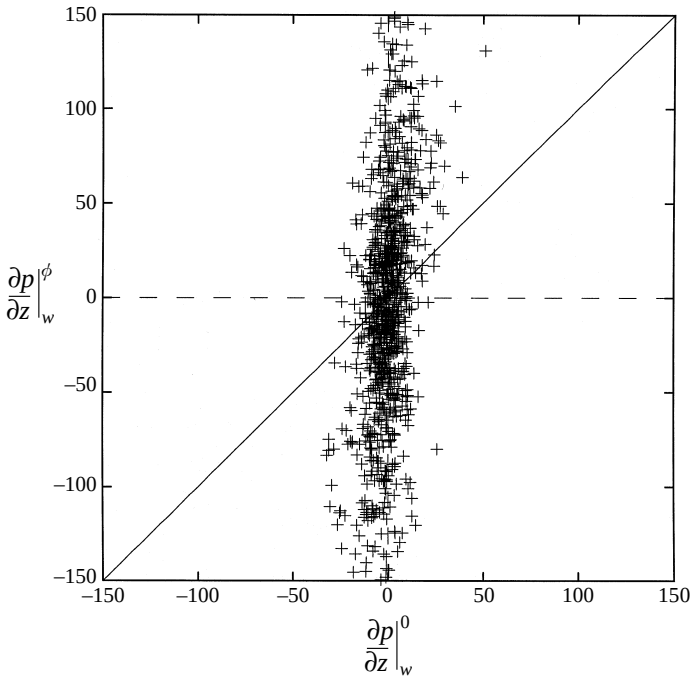

FIGURE 2. Correlation between a pressure field of a no-control case and a pressure field modified by a control based on information at $y^+ = 10$. A line indicating no change of the pressure field is drawn for guidance.

motion induced by the vortex. This blowing and suction creates locally high pressure in the near-wall region marked with '+', and low pressure in the region marked with '−' in figure 1. A crucial aspect of the present analysis is the observation that this blowing and suction *increases* the pressure gradient in the spanwise direction under the streamwise vortex near the wall. To demonstrate this behaviour, we examine computed flow fields. Figure 2 shows a scatter plot between two pressure gradient fields: $\partial p/\partial z|_w^0$ is the pressure gradient before the control is applied and $\partial p/\partial z|_w^{\phi}$ is the pressure gradient at the same location after the control of Choi *et al.* (1994) is applied for one time step. It is apparent that the control increased the pressure gradient significantly. For the uncontrolled case, Re_τ based on the wall-shear velocity and the channel half-width is about 110. The spectral code of Kim, Moin & Moser (1987) is used for all the computations presented here. Simulations are carried out

using $32 \times 65 \times 32$ spectral modes (with dealiasing in the streamwise and spanwise directions) with the computational domain of $4\pi\delta \times 2\delta \times 4\pi\delta/3$, respectively.

The above argument suggests that we should seek blowing and suction that increases the pressure gradient in the spanwise direction near the wall for a short time period (i.e. in the suboptimal sense) in order to achieve a similar drag reduction to that achieved by Choi *et al.*'s (1994) control. The cost functional $\mathscr{J}(\phi)$ to be minimized is then

$$\mathscr{J}(\phi) = \frac{\ell}{2A\Delta t}\int_S\int_t^{t+\Delta t} \phi^2 \,\mathrm{d}t\,\mathrm{d}S - \frac{1}{2A\Delta t}\int_S\int_t^{t+\Delta t}\left(\frac{\partial p}{\partial z}\right)_w^2 \mathrm{d}t\,\mathrm{d}S, \tag{2.4}$$

where the integrations are over the wall (S) in space and over a short duration in time Δt, which typically corresponds to the time step used in the numerical computation, and ℓ is the relative price of the control since the first term on the right-hand side represents the cost of the actuation ϕ. Note that there is a minus sign in front of the second term since we want to maximize the pressure gradient. It should be noted that the spanwise pressure gradient at the wall will be eventually reduced when the strength of the near-wall streamwise vortices is reduced through successful control. Here, blowing and suction that increase the spanwise pressure gradient for the next step are sought as a suboptimal control.

To minimize the cost functional, we first define the differential states of the velocity and pressure, (θ_i, ρ), using a Fréchet differential (Finlayson 1972),

$$\theta_i = \frac{\mathscr{D}u_i(\phi)}{\mathscr{D}\phi}\tilde{\phi}, \tag{2.5}$$

$$\rho = \frac{\mathscr{D}p}{\mathscr{D}\phi}\tilde{\phi}, \tag{2.6}$$

where

$$\frac{\mathscr{D}f(\phi)}{\mathscr{D}\phi}\tilde{\phi} = \lim_{\epsilon\to 0}\frac{f(\phi+\epsilon\tilde{\phi}) - f(\phi)}{\epsilon}, \tag{2.7}$$

$\tilde{\phi}$ being an arbitrary perturbation field to ϕ.

Next, we choose the Crank–Nicolson scheme for the linear terms and a Runge–Kutta scheme for the nonlinear terms to yield a discretized form of (2.1) and (2.2):

$$u_i^{n+1} - \frac{\Delta t}{2Re}\frac{\partial^2 u_i^{n+1}}{\partial x_j \partial x_j} + \frac{\Delta t}{2}\frac{\partial p^{n+1}}{\partial x_i} + R^n = 0, \tag{2.8}$$

$$\frac{\partial u_j^{n+1}}{\partial x_j} = 0, \tag{2.9}$$

with

$$u_i^{n+1}|_w = \phi\ \delta_{i2}, \tag{2.10}$$

where the superscripts $n+1$ and n denote the time step, and R^n includes the nonlinear terms and the explicit parts of the pressure gradient and viscous terms. The Fréchet differential of (2.8)-(2.10) yields the governing equations for the differential states (θ_i, ρ),

$$\theta_i^{n+1} - \frac{\Delta t}{2Re}\frac{\partial^2 \theta_i^{n+1}}{\partial x_j \partial x_j} + \frac{\Delta t}{2}\frac{\partial \rho^{n+1}}{\partial x_i} = 0, \tag{2.11}$$

$$\frac{\partial \theta_j^{n+1}}{\partial x_j} = 0, \tag{2.12}$$

with

$$\theta_i^{n+1}|_w = \tilde{\phi}\ \delta_{i2}. \tag{2.13}$$

Note that $(\mathscr{D}R^n/\mathscr{D}\phi)\ \tilde{\phi} = 0$. Hereinafter, we drop the superscript $n+1$ and all variables are understood to be at the $(n+1)$th time step. Note that there is no contribution from the nonlinear terms, thus making the equations linear. Generally, the suboptimal formulation depends on the time advancement scheme used, as shown here (see also Choi *et al.* 1993). Dropping the nonlinear terms may miss important flow dynamics. However, we found from our numerical tests with the full nonlinear terms included that the contribution from the nonlinear terms is negligible in our boundary control with short optimization interval Δt; it turns out that the conservation of mass due to the wall actuation dominates the near-wall dynamics.

Under the approximation that $2Re/\Delta t \gg k^2$, where $k = (k_x^2 + k_z^2)^{1/2}$, and k_x and k_z denote the streamwise and spanwise wavenumbers in the x- and z-directions respectively†, the above equations have the following solutions in the semi-infinite domain with periodic conditions in the x- and z-directions (see the Appendix):

$$\hat{\theta}_1(y) = \frac{\mathrm{i}k_x}{k}\hat{\tilde{\phi}}\left(\exp[-(2Re/\Delta t)^{1/2}y] - \mathrm{e}^{-ky}\right), \tag{2.14}$$

$$\hat{\theta}_3(y) = \frac{\mathrm{i}k_z}{k}\hat{\tilde{\phi}}\left(\exp[-(2Re/\Delta t)^{1/2}y] - \mathrm{e}^{-ky}\right), \tag{2.15}$$

$$\hat{\theta}_2(y) = \hat{\tilde{\phi}}\mathrm{e}^{-ky}, \tag{2.16}$$

$$\hat{\rho}(y) = \frac{2}{k\ \Delta t}\hat{\tilde{\phi}}\mathrm{e}^{-ky}, \tag{2.17}$$

where $\hat{\theta}_j, \hat{\rho}$, and $\hat{\tilde{\phi}}$ are the Fourier coefficients of θ_j, ρ, and $\tilde{\phi}$ respectively. For the channel geometry, we originally considered both walls and found that the interaction between two walls is negligible as long as the typical wavelength ($\sim 2\pi/k$) associated with near-wall structures is much smaller than the channel width.

The Fréchet differential of the cost functional (2.4) becomes

$$\frac{\mathscr{D}\mathscr{J}}{\mathscr{D}\phi}\tilde{\phi} = \frac{\ell}{A\Delta t}\int_S\int_t^{t+\Delta t}\phi\tilde{\phi}\ \mathrm{d}t\ \mathrm{d}S - \frac{1}{A\Delta t}\int_S\int_t^{t+\Delta t}\left.\frac{\partial p}{\partial z}\right|_w\left.\frac{\partial \rho}{\partial z}\right|_w\ \mathrm{d}t\ \mathrm{d}S. \tag{2.18}$$

The Fourier representation of the above equation is

$$\widehat{\frac{\mathscr{D}\mathscr{J}}{\mathscr{D}\phi}}\hat{\tilde{\phi}}^* = \ell\hat{\phi}\hat{\tilde{\phi}}^* - \left.\widehat{\frac{\partial p}{\partial z}}\right|_w\left.\widehat{\frac{\partial \rho}{\partial z}}^*\right|_w, \tag{2.19}$$

where the hat denotes the Fourier coefficient, and the superscript $*$ denotes the complex conjugate. From (2.17), $\widehat{\partial\rho/\partial z}^*|_w$ can be expressed in terms of $\hat{\tilde{\phi}}^*$,

$$\left.\widehat{\frac{\partial \rho}{\partial z}}^*\right|_w = -\frac{2\mathrm{i}k_z}{k\ \Delta t}\hat{\tilde{\phi}}^*. \tag{2.20}$$

Equation (2.19) then reduces to

$$\widehat{\frac{\mathscr{D}\mathscr{J}}{\mathscr{D}\phi}}\hat{\tilde{\phi}}^* = \ell\hat{\phi}\hat{\tilde{\phi}}^* - \frac{2k_z^2}{k\ \Delta t}\hat{p}_w\hat{\tilde{\phi}}^*. \tag{2.21}$$

† It can be shown that $2Re/\Delta t k_{max}^2 \sim Re^{1/4} \gg 1$. Here we used $u\Delta t/\Delta x \sim O(1)$ and $k_{max} \sim k_\eta \sim Re^{3/4}$, where k_η is the wavenumber corresponding to the Kolmogorov length scale.

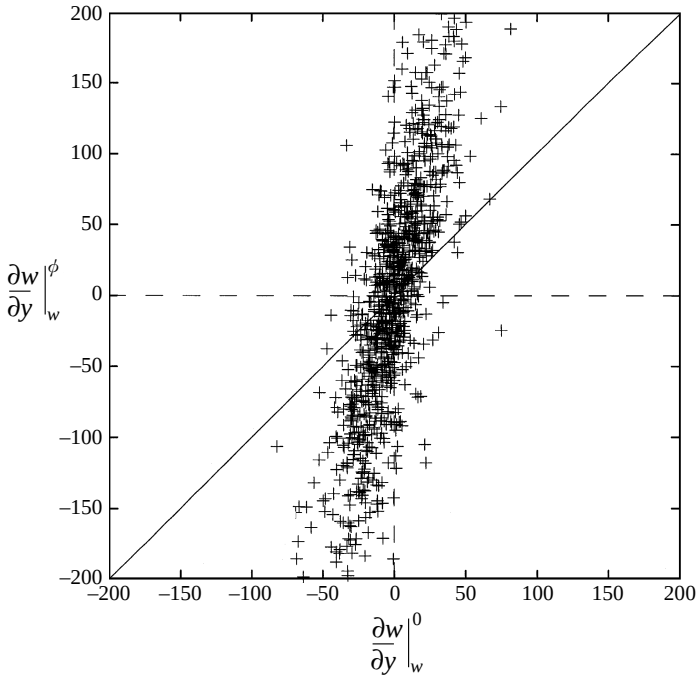

FIGURE 3. Correlation between a spanwise wall-shear stress of a no-control case and a spanwise wall-shear stress modified by a control based on $y^+ = 10$. A line indicating no change of the spanwise wall-shear stress field is drawn for guidance.

For an arbitrary $\hat{\tilde{\phi}}$, equation (2.21) should be satisfied, yielding

$$\widehat{\frac{\mathscr{D}\mathscr{J}}{\mathscr{D}\phi}} = \ell\hat{\phi} - \frac{2k_z^2}{k\Delta t}\hat{p}_w. \tag{2.22}$$

From the requirement that the Fréchet differential of the cost functional be minimized, i.e. $\mathscr{D}\mathscr{J}/\mathscr{D}\phi = 0$, the optimum $\hat{\phi}$ then becomes

$$\hat{\phi} = C\frac{k_z^2}{k}\hat{p}_w, \tag{2.23}$$

where C is a positive scale factor that determines the cost of the actuation. Equation (2.23) indicates that the optimum wall actuation is negatively proportional to the second spanwise derivative of the wall pressure, with the high-wavenumber components reduced by $1/k$.

Another wall quantity that indicates similar changes of the near-wall dynamics due to the altered pressure field is the spanwise shear at the wall, $\partial w/\partial y$. Owing to the added pressure gradient in the spanwise direction below the streamwise vortex, the spanwise flow near the wall is also induced, thus increasing the spanwise shear stress at the wall (see figure 1). The scatter plot between the spanwise shear stress at the wall from two different fields, one of which is from an unperturbed channel and the other with the control based on $y^+ = 10$, is shown in figure 3. Thus another choice for the cost functional to be minimized is

$$\mathscr{J}(\phi) = \frac{\ell}{2A\Delta t}\int_S\int_t^{t+\Delta t}\phi^2\,\mathrm{d}t\,\mathrm{d}S - \frac{1}{2A\Delta t}\int_S\int_t^{t+\Delta t}\left(\frac{\partial w}{\partial y}\right)_w^2\,\mathrm{d}t\,\mathrm{d}S\,. \tag{2.24}$$

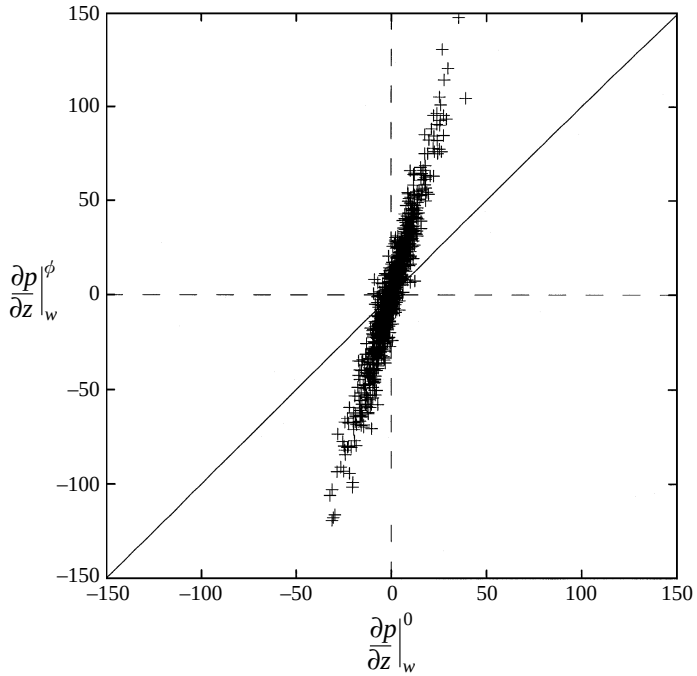

FIGURE 4. Correlation between a pressure field of a no-control case and a pressure field modified by a control based on equation (2.23).

Following the procedure that led to equation (2.23) yields the optimum actuation:

$$\hat{\phi} = C\frac{ik_z}{k}\left.\widehat{\frac{\partial w}{\partial y}}\right|_w . \tag{2.25}$$

Equation (2.25) indicates that the optimum wall actuation should be proportional to the spanwise derivative of the spanwise shear at the wall, with the high-wavenumber components reduced by $1/k$. Note that the scale factor C in equations (2.23) and (2.25) is arbitrary. As mentioned before, the suboptimal formulation depends on the time-advancement scheme used. However, if we used a different implicit scheme, only the resulting constant C would be different. This does not cause a problem since C is chosen such that the r.m.s. value of the wall actuation is maintained at a given value.

In the following simulations, we set the r.m.s. value of ϕ to be equal to that of the wall-normal velocity at $y^+ = 10$, which gives the same r.m.s. value of wall actuations as that of Choi *et al.* (1994).

3. Results

The above control laws (2.23) and (2.25) are tested in a turbulent channel flow. The pressure gradient at the wall is monitored to see if the equation (2.23) control increases the pressure gradient when the control law is applied. It behaves as expected, as shown in figure 4. The spanwise shear stress at the wall also increases when the equation (2.25) control is applied (see figure 5). These results also confirm that a suboptimal procedure without the nonlinear terms does not cause an error for our

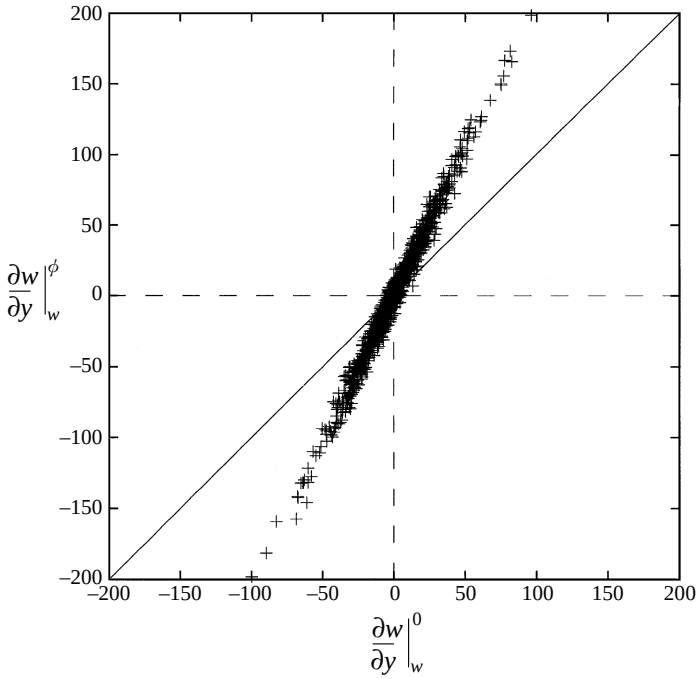

FIGURE 5. Correlation between a spanwise wall-shear stress of a no-control case and a spanwise wall-shear stress modified by a control based on equation (2.25).

boundary controls. Since these control laws specifically increase the wall pressure gradient or spanwise wall-shear stress, correlations between these variables before and after control are much higher than those corresponding to the control based on $y^+ = 10$ information. This suggests that the controls based on equations (2.23) and (2.25) modify the flow in a different manner from the control based on information at $y^+ = 10$.

Time histories of the mean streamwise wall-shear stress for different control laws are shown in figures 6 and 7. As control begins, an immediate drop in the shear stress is observed for all cases. At the same expense (i.e. the same r.m.s. value of ϕ), the control based on (2.25), which reduces drag by as much as 22%, is apparently more effective than that based on (2.23) which reduces drag by 16%. This indicates that the spanwise wall-shear stress is a better quantity for control input.

The control laws presented above, however, are still impractical to implement, since they are expressed in terms of the Fourier coefficients (i.e. in wavenumber space), which require information over the entire spatial domain. Therefore, the inverse transforms of k_z^2/k and ik_z/k are sought numerically so that the convolution integral can be used to express the control laws in physical space. The discrete representation of each control law then becomes†:

$$\phi(x_j, z_k) = C \sum_{j'} \sum_{k'} W^p_{j'k'} p_w(x_{j+j'}, z_{k+k'}) \tag{3.1}$$

† Since k_z^2/k and ik_z/k are not periodic in the wavenumber space, a high resolution was used to obtain W^p_{jk} and W^w_{jk} to minimize aliasing error.

		$k(=z/\Delta z)$						
		0	1	2	3	4	5	6
	0	**1.0000**	**−0.4427**	**0.0031**	**−0.0440**	**0.0044**	**−0.0138**	**0.0032**
$j(=x/\Delta x)$	1	**0.0413**	**−0.0007**	**−0.0040**	**−0.0037**	**−0.0029**	**−0.0021**	−0.0016
	2	**−0.0110**	0.0057	0.0019	0.0011	0.0002	0.0000	−0.0003

TABLE 1. The weight distribution of equation (3.1), W^p_{jk}. The weights are symmetric between j and $-j$ and k and $-k$. The weights are normalized by W^p_{00}. Bold faced weights are used in the calculation of figure 6. Here, $\Delta x^+ = 40$ and $\Delta z^+ = 13$ ($\Delta x = 3\Delta z$).

		$k(=z/\Delta z)$						
		0	1	2	3	4	5	6
	0	**0.0000**	**1.0000**	**−0.1039**	**0.2679**	**−0.0852**	**0.1419**	−0.0671
$j(=x/\Delta x)$	1	0.0086	0.0537	0.0503	0.0310	0.0340	0.0148	0.0237
	2	0.0001	−0.0104	0.0059	0.0051	0.0100	0.0074	0.0092

TABLE 2. The weight distribution of equation (3.2), W^w_{jk}. The weights are symmetric between j and $-j$ and antisymmetric between k and $-k$. The weights are normalized by W^w_{01}. Bold faced weights are used in the calculation of figure 7. Here, $\Delta x^+ = 40$ and $\Delta z^+ = 13$ ($\Delta x = 3\Delta z$).

and

$$\phi(x_j, z_k) = C \sum_{j'} \sum_{k'} W^w_{j'k'} \left. \frac{\partial w}{\partial y} \right|_w (x_{j+j'}, z_{k+k'}), \tag{3.2}$$

respectively. The subscripts, j and k, denote the discretizing indices in the x- and z-directions respectively. The weights, W^p_{jk} and W^w_{jk}, are given in tables 1 and 2. Note that the weights decay rapidly with distance from the point of interest, suggesting that the optimum actuation can be obtained by a local weighted average of the pressure or spanwise shear stress. The results obtained using a 37-point average for the pressure and an 11-point average for the spanwise shear stress yield about the same drag reduction as that obtained from full integration using equations (2.23) and (2.25) (see figures 6 and 7). The weights used in these calculations are bold-faced in tables 1 and 2. It is remarkable that localized information can produce such a significant drag reduction, especially for the control with the spanwise shear stress.

The weight distribution W^w_{jk} for $j = 0$ is very similar to the one found in the application of neural networks to the same turbulent flow (Lee *et al.* 1997), in which only a single strip of the spanwise shear information was used in the network. The control law of Lee *et al.*,

$$\hat{\phi} = C \frac{\mathrm{i}k_z}{|k_z|} \left. \widehat{\frac{\partial w}{\partial y}} \right|_w, \tag{3.3}$$

produces almost the same distribution of blowing and suction as the present results. Note that blowing and suction from equation (2.25) are nearly the same as those from equation (3.3) because the near-wall structures have relatively slow variation in the streamwise direction (the $k_x = 0$ component is dominant). This blowing and suction distribution is also very similar to the one based on $y^+ = 10$ data (see Lee *et al.* 1997).

In figure 8, contours of the streamwise vorticity in a cross-flow plane for the control with equation (2.25) are compared with a no-control case. Significant reduction in

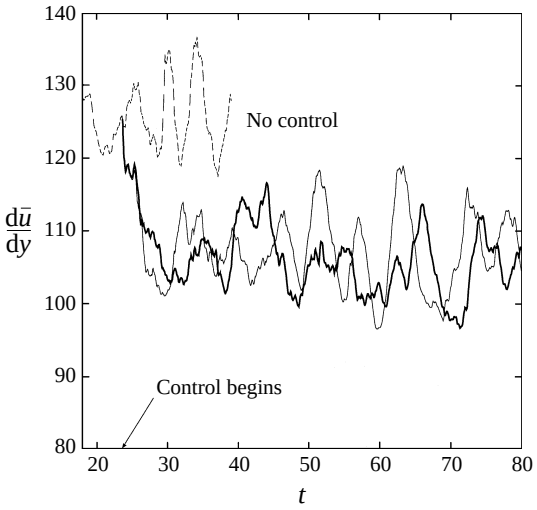

FIGURE 6. Mean streamwise wall-shear stress for various control laws based on the wall pressure, compared to the no-control case: thick solid line, the control law expressed in Fourier space, equation (2.23); thin solid line, the control law expressed in physical space, equation (3.1) with the integration radius of $6\Delta z$. $\Delta t^+ \simeq 0.2$.

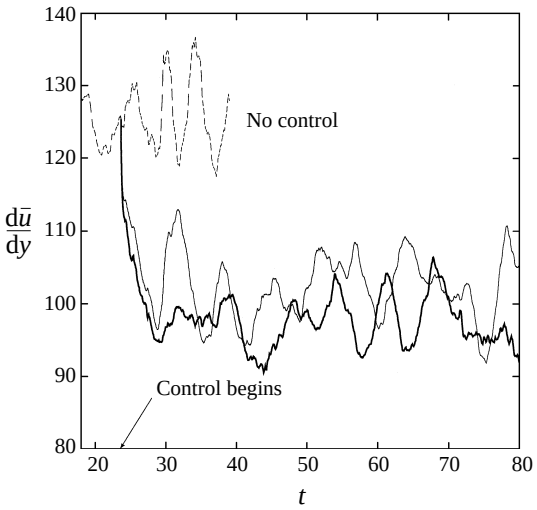

FIGURE 7. Mean streamwise wall-shear stress for various control laws based on the spanwise wall-shear stress compared to the no-control case: thick solid line, the control law expressed in Fourier space, equation (2.25); thin solid line, the control law expressed in physical space, equation (3.2) with 11 points in the spanwise direction only. $\Delta t^+ \simeq 0.2$.

the strength of the streamwise vortices is evident. This again confirms the notion that a successful manipulation of the near-wall streamwise vortices can lead to drag reduction. The mean streamwise velocity and root-mean-square velocity near the wall are shown in figures 9 and 10, respectively, and compared with the no-control case. The trends are very similar to Choi *et al.* (1994) and Lee *et al.* (1997).

Finally, we mention that we tried to find a feedback control scheme minimizing the

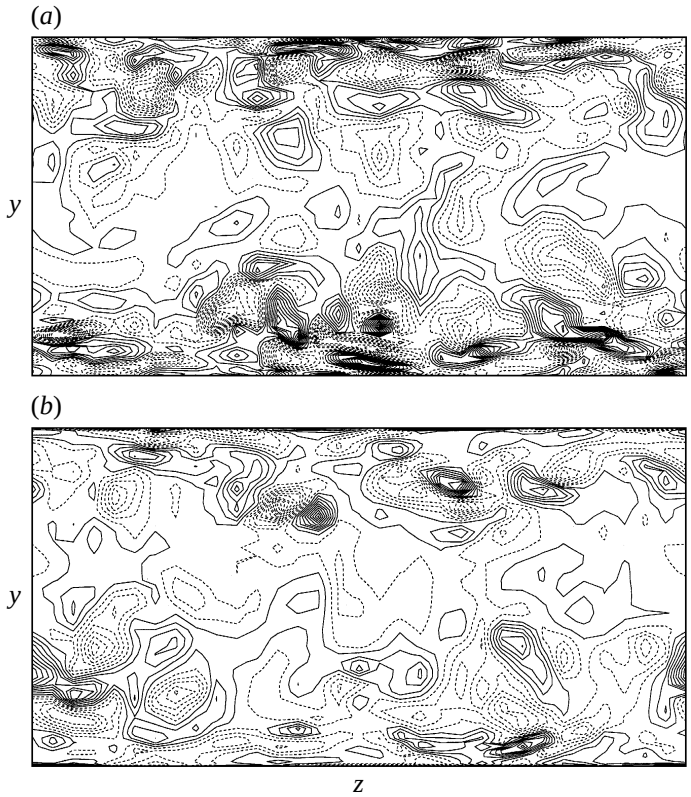

FIGURE 8. Contours of the streamwise vorticity in a cross-flow plane: (*a*) no control; (*b*) control based on wall-shear stress (equation (2.25)). The contour level increment is the same for both figures. Negative contours are dashed.

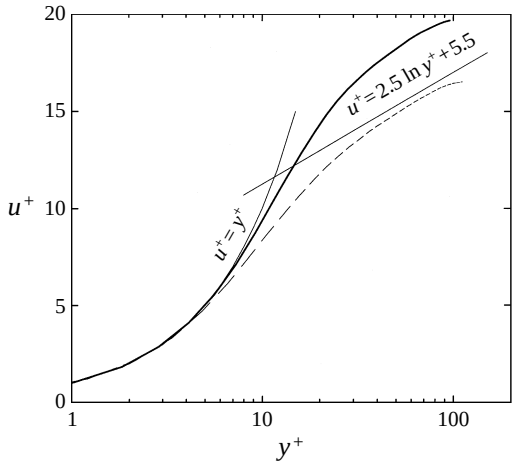

FIGURE 9. The mean streamwise velocity normalized by u_τ: Thick solid line, control law (2.25); dashed line, no control. For the controlled case, the velocity is normalized by the controlled u_τ.

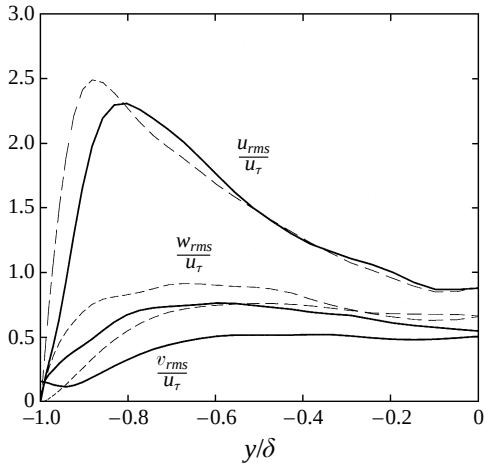

FIGURE 10. The root-mean-square velocity normalized by u_τ of the uncontrolled flow: thick solid line, control law (2.25); dashed line, no control.

following cost functional:

$$\mathscr{J}(\phi) = \frac{\ell}{2A\Delta t}\int_S\int_t^{t+\Delta t}\phi^2\,\mathrm{d}t\,\mathrm{d}S + \frac{1}{2A\Delta t}\int_S\int_t^{t+\Delta t}\left(\frac{\partial u}{\partial y}\right)_w^m\,\mathrm{d}t\,\mathrm{d}S, \tag{3.4}$$

with $m = 1$ or 2. This cost functional is the most natural choice since it contains the quantity directly related to drag. We followed the same procedure to derive the following control schemes:

$$\hat{\phi} = 0, \tag{3.5}$$

for $m = 1$, and

$$\hat{\phi} = -C\frac{\mathrm{i}k_x}{k}\left.\widehat{\frac{\partial u}{\partial y}}\right|_w, \tag{3.6}$$

for $m = 2$. Equation (3.5) obviously does not reduce drag and equation (3.6) increased drag in our numerical simulations. This failure appears to be due to the neglect of the nonlinear terms in our formulation, since the numerical solution of the optimum wall actuations with the full nonlinear terms gave different results (Bewley & Moin 1994). This suggests that even in a short time interval the nonlinear terms should be included in the suboptimal formulation when drag itself is chosen as the cost functional. Manipulation of the streamwise vortices by wall actuation, however, can be accomplished through a linear process as shown in the previous section. It appears that having a term that is directly related to near-wall streamwise vortices in the cost functional indirectly includes the nonlinear effect. This is probably related to the fact that near-wall streamwise vortices are self-sustained by a nonlinear process (Hamilton, Kim & Waleffe 1995). If the nonlinear terms are included, of course, it is impossible to derive the feedback control law in closed form without approximation. Hill (1993), on the other hand, considered the nonlinear term by modelling the near-wall flow using the Taylor series expansion and presented a feedback control law in closed form, which resulted in about 15% drag reduction.

4. Summary

We have obtained two simple feedback control laws for drag reduction by applying a suboptimal control procedure to a turbulent flow. This was possible since we selected two cost functionals guided by the successful control based on quantities monitored at $y^+ = 10$. The present control laws perform very well, resulting in substantial drag reductions when applied to a turbulent channel flow. More convenient control schemes requiring only local information were also derived, and were shown to work equally well. They require quantities measurable only at the surface and thus should be easier to implement in practice. The present results further substantiate the notion that a successful manipulation of the near-wall streamwise vortices is the key to boundary-layer control for drag reduction.

We are grateful to Dr Gary Coleman and Mr Hong Zhang for useful discussions. This work was supported by AFOSR grant F49620-95-10263 (Program Managers, Drs James M. McMichael and Marc N. Glauser). Computer time was provided by the NAS Program of NASA Ames Research Center, the San Diego Supercomputer Center, and the DoD High Performance Computing Center. H.C. acknowledges the support by KOSEF through Turbo and Power Machinery Research Center.

Appendix. Derivation of the solution (2.14)–(2.17)

Equations for the differential states (θ_i, ρ), (2.11), (2.12) can be rewritten in terms of the Fourier coefficients,

$$\hat{\theta}_1 - \frac{\Delta t}{2Re}\left(\frac{\mathrm{d}^2}{\mathrm{d}y^2} - k^2\right)\hat{\theta}_1 + \frac{\mathrm{i}k_x \Delta t}{2}\hat{\rho} = 0, \tag{A 1}$$

$$\hat{\theta}_2 - \frac{\Delta t}{2Re}\left(\frac{\mathrm{d}^2}{\mathrm{d}y^2} - k^2\right)\hat{\theta}_2 + \frac{\Delta t}{2}\frac{\mathrm{d}\hat{\rho}}{\mathrm{d}y} = 0, \tag{A 2}$$

$$\hat{\theta}_3 - \frac{\Delta t}{2Re}\left(\frac{\mathrm{d}^2}{\mathrm{d}y^2} - k^2\right)\hat{\theta}_3 + \frac{\mathrm{i}k_z \Delta t}{2}\hat{\rho} = 0, \tag{A 3}$$

$$\mathrm{i}k_x\hat{\theta}_1 + \mathrm{i}k_z\hat{\theta}_3 + \frac{\mathrm{d}\hat{\theta}_2}{\mathrm{d}y} = 0, \tag{A 4}$$

with

$$\hat{\theta}_i(0) = \hat{\bar{\phi}}\delta_{i2}, \qquad \hat{\theta}_i(\infty) = 0, \tag{A 5}$$

where $\hat{\theta}_i$ and $\hat{\rho}$ are defined as follows:

$$\theta_i = \sum_{k_x}\sum_{k_z}\hat{\theta}_i(y)\mathrm{e}^{\mathrm{i}k_x x}\mathrm{e}^{\mathrm{i}k_z z}, \tag{A 6}$$

$$\rho = \sum_{k_x}\sum_{k_z}\hat{\rho}(y)\mathrm{e}^{\mathrm{i}k_x x}\mathrm{e}^{\mathrm{i}k_z z}. \tag{A 7}$$

The operation $\mathrm{i}k_x\cdot$ (A 1) $+\mathrm{d}/\mathrm{d}y$(A 2) $+\mathrm{i}k_z\cdot$ (A 3) together with equation (A 4) yields

$$\frac{\mathrm{d}^2\hat{\rho}}{\mathrm{d}y^2} - k^2\hat{\rho} = 0, \tag{A 8}$$

which has a non-growing solution,

$$\hat{\rho} = \hat{\rho}_w\mathrm{e}^{-ky}, \tag{A 9}$$

with a wall value, $\hat{\rho}_w$, which will be determined later. Using (A 9), we can find solutions to equations (A 1), (A 2), (A 3),

$$\hat{\theta}_1(y) = \frac{\Delta t}{2} \mathrm{i} k_x \hat{\rho}_w \left(\exp[-(k^2 + 2Re/\Delta t)^{1/2} y] - \mathrm{e}^{-ky} \right), \tag{A 10}$$

$$\hat{\theta}_3(y) = \frac{\Delta t}{2} \mathrm{i} k_z \hat{\rho}_w \left(\exp[-(k^2 + 2Re/\Delta t)^{1/2} y] - \mathrm{e}^{-ky} \right), \tag{A 11}$$

$$\hat{\theta}_2(y) = \left(\hat{\hat{\phi}} - \frac{\Delta t}{2} k \hat{\rho}_w \right) \exp[-(k^2 + 2Re/\Delta t)^{1/2} y] + \frac{\Delta t}{2} k \hat{\rho}_w \mathrm{e}^{-ky}. \tag{A 12}$$

With these, equation (A 4) reduces to

$$\left(- \left(k^2 + \frac{2Re}{\Delta t} \right)^{1/2} \left(\hat{\hat{\phi}} - \frac{\Delta t}{2} k \hat{\rho}_w \right) - \frac{\Delta t}{2} k^2 \hat{\rho}_w \right) \exp[-(k^2 + 2Re/\Delta t)^{1/2} y] = 0. \tag{A 13}$$

Since $2Re/\Delta t \gg k^2$, equation (A 13) yields

$$\hat{\rho}_w = \frac{2}{\Delta t \, k} \hat{\hat{\phi}}. \tag{A 14}$$

With this, equations (A 10), (A 11), (A 12), (A 9) become equations (2.14), (2.15), (2.16), (2.17), respectively.

REFERENCES

Abergel, F. & Temam, R. 1990 On some control problems in fluid mechanics. *Theor. Comput Fluid Dyn.* **1**, 303.

Bewley, T. & Moin, P. 1994 Optimal control of turbulent channel flows. In *Active Control of Vibration and Noise* (ed. K. W. Wang, A. H. Von Flotow, R. Shoureshi, E. W. Hendricks & T. W. Farabee). ASME DE-Vol. 75.

Choi, H., Moin, P. & Kim, J. 1994 Active turbulence control for drag reduction in wall-bounded flows. *J. Fluid Mech.* **262**, 75.

Choi, H., Temam, R., Moin, P. & Kim, J. 1993 Feedback control for unsteady flow and its application to the stochastic Burgers equation. *J. Fluid Mech.* **245**, 509.

Finlayson, B. A. 1972 *The Method of Weighted Residuals and Variational Principles.* Academic.

Hamilton, J. M., Kim, J. & Waleffe, F. 1995 Regeneration mechanisms of near-wall turbulence structures. *J. Fluid Mech.* **287**, 317.

Hill, D. C. 1993 Drag reduction at a plane wall. *Annual Research Briefs.* Center for Turbulence Research, Stanford University.

Hill, D. C. 1994 Drag reduction strategies. *Annual Research Briefs.* Center for Turbulence Research, Stanford University.

Kim, J., Moin, P. & Moser, R. 1987 Turbulence statistics in fully developed channel flow at low Reynolds number. *J. Fluid Mech.* **177**, 133.

Lee, C., Kim, J., Babcock, D. & Goodman, R. 1997 Application of neural networks to turbulence control for drag reduction. *Phys. Fluids* **9**, 1740.